,,amsmath

[SSC24-X-X]

[MeV gamma-ray detector on the 50-kg class satellite]

K. S. Tanaka, J. Kataoka, R. Iwashita, R. Mori, T. Suga, S. Ogasawara, M. Tao
Waseda University,
Faculty of Science and Engineering, 3-4-1 Okubo, Shinjuku-ku, Tokyo, 169-8555, Japan
tanaka@kaduo.jp

Y. Yatsu, C. Toshihiro
Tokyo Institute of Technology,
2-12-1 Ookayama, Meguro-ku, Tokyo, 152-8550, Japan

S. Takeda, M. Onishi
iMAGINE-X Inc.,
1-12-8 Shibuya, Shibuya-ku, Tokyo, 150-0002, Japan

ABSTRACT

We are planning to launch a 50kg-class satellite named GRAPHIUM, equipped with a small, high-performance Hybrid Compton Camera (INSPIRE) for MeV gamma-ray astronomy.Since the launch of the COMPTEL satellite in 1991, there have been limited observations in the MeV gamma-ray band. However, this energy range is crucial for studying nucleosynthesis processes. GRAPHIUM aims to conduct a wide-area survey of nuclear gamma rays from the galactic plane and includes gamma-ray observations of solar flares as one of its objectives. Equipped with a hybrid Compton camera system, GRAPHIUM can perform simultaneous X-ray and gamma-ray imaging. This is achieved by integrating the features of both Compton and pinhole cameras within a single detector system. The system includes two sensor layers of large-area Silicon Photomultiplier (SiPM) arrays, optically coupled with GAGG scintillators. This configuration enables simultaneous imaging of gamma rays from 30 to 200 keV in pinhole mode and from 200 to 3000 keV in Compton mode. Regarding the Engineering Model of this detector, each layer's two-dimensional imaging was evaluated using a source. Additionally, temperature resistance and radiation resistance tests were conducted on the data acquisition board. Additionally, temperature resistance and radiation resistance tests were conducted on the data acquisition board. The GRAPHIUM satellite is being developed as the successor to PETREL, which is currently being prepared for launch, with a planned launch in 2027.

1 INTRODUCTION

In the MeV gamma-ray range, various radiative processes occur in space, including line gamma rays and electron-positron annihilation lines associated with the decay of radioactive isotopes and nuclear de-excitation. These processes serve as important observational targets for probing nucleosynthesis in the universe.

Heavy elements such as gold and platinum are believed to be produced by the r-process, which involves rapid neutron capture followed by beta decay. This process occurs only in regions with abundant high-temperature neutrons. Recent observations of gravitational waves and electromagnetic signals suggest that kilonovae, resulting from supernova explosions or neutron star mergers, are promising candidates for r-process sites.[1] Direct observation of gamma rays, such as the 412 keV line from ^{197}Au, from these phenomena would provide solid evidence of heavy element production in neutron-rich regions.

Despite their potential as probes to explore various nucleosynthesis mechanisms and astronomical phenomena, only about 30 steady celestial sources were discovered by COMPTEL, launched in 1991.[2] Nuclear gamma-ray maps from isotopes like ^{26}Al were obtained by COMPTEL,[3] but no observations with sensitivity exceeding COMPTEL's have been made since then.

Observing MeV gamma rays is challenging because these rays do not reach the ground, necessitating satellite observations. Using focusing systems

like those for visible light or soft X-rays is difficult, and since Compton scattering is the primary interaction with matter, the Compton camera method is employed. However, statistical methods are required to determine the arrival direction, making high S/N ratio observations challenging.

In this context, we plan to launch a 50kg-class satellite equipped with a small, high-performance Hybrid Compton Camera (INSPIRE) to scan the galactic plane and elucidate the mechanisms of nucleosynthesis in the universe.[4,5]

The small satellite GRAPHIUM, which will carry this detector, is being developed in collaboration with the satellite group at Tokyo Institute of Technology, utilizing their expertise in satellite bus design. This group has previously launched and operated HIBARI[6,7] and is planning the launch of PETREL.[8] These satellites feature VSAC (Variable Shape Attitude Control), allowing maneuvers using paddles to change shape without relying on thrusters.

2 Hybrid Compton Camera

The INSPIRE under development features a detector area of 100 cm^2 and an estimated weight of 9935 g. The dimensions of the detector unit are 1874 mm $\times$ 1874 mm $\times$ 1124 mm, and it is designed to be installed within the separation system of the GRAPHIUM satellite (Fig. 1). The fundamental design leverages our expertise in detection technologies used for simultaneous X-ray and gamma-ray imaging across various fields, including medical applications.[9,10]

The detector section is composed of scatterers, bottom absorbers, and side absorbers. These units are arranged in a 2×2 configuration for both the scatterer and the absorber, with two units per side, forming a box-type detector. The scatterers and absorbers are positioned 50 mm apart.

The scatterer and side absorbers measure 50 mm $\times$ 50 mm $\times$ 5 mm and feature a 45×45 pixel scintillator array. The scatterer includes a central 5.5 mm hole for pinhole mode. The bottom absorber is 50 mm$\times$50 mm$\times$20 mm and has a 23×23 pixel 3D position detection structure (Depth-of-Interaction: DOI).

Each unit is composed of pixelated GAGG scintillators and Multi-Pixel Photon Counter (MPPC) arrays, optically bonded via 1 mm thick light guides. Low-energy gamma rays are detected in pinhole mode, while high-energy gamma rays are detected in Compton mode, covering the range from 30 keV to 3 MeV.

The detector is surrounded by Bi4Ge3O12 (BGO) scintillators for background and escape event rejection, which are read out by 6 mm square single-element MPPCs.

The MPPC arrays consist of 256 channels (16 ch$\times$16 ch), with the scatterer using S14161-1685 (50 μm) and the absorbers and sides using S14161-2109 (50 μm pitch). Signals read from the four edges are used to determine the 2D interaction position via centroid calculation.

Low-energy gamma rays, which are primarily absorbed by photoelectric absorption, are imaged using the pinhole camera principle. The scatterer includes four holes, each geometrically aligned with the absorber directly behind it, allowing for unique determination of gamma-ray arrival directions. For gamma rays above several hundred keV, Compton scattering in the scatterer and photoelectric absorption in the absorber restrict the gamma-ray arrival direction. The box-type detector selects events where combinations of scatterer and bottom absorber or scatterer and side absorber are detected. This setup allows the side absorber to improve the field of view by being added to the conventional Compton camera configuration (a combination of scatterer and bottom absorber).

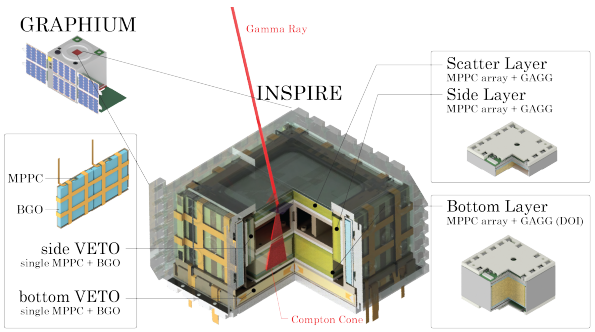

Figure 1: Diagram of the INSPIRE installed on the GRAPHIUM satellite. It is placed inside the separation system of the satellite and consists of the scatterer, side absorber, and bottom absorber, each composed of GAGG scintillators and MPPCs. The detector is surrounded by BGO scintillators for background and escape event rejection, read out by 6 mm square single-element MPPCs.

3 Data Acquisition System

The data processing system of the INSPIRE is shown in Fig.2. Signals from the MPPCs are sent to six ADC boards via flat flexible cables. The ADC boards amplify, shape, and digitize the signals be-

Table 1: Specifications of the INSPIRE and satellite integration requirements

Size	1874 mm × 1874 mm × 1124 mm
Weight	9935 g (without DAQ)
Power	Steady 21 W, Max 24 W
Field of View	± 30 degrees (Pinhole), ± 60 degrees (Compton)
Mission Duration	> 2 years
Data Transfer Volume	< 1 GByte / day
Observation Time	∼ 30 min / orbit

fore sending them to the FPGA on the USB board via UART, along with clock information.

The data on the FPGA buffer is extracted by the Raspberry Pi via USB Bulk transfer and saved to the SSD drive connected to the Raspberry Pi as 13 byte packets containing the analog board number, clock, and ADC values. This system can acquire and save data at a maximum event rate of about 80 K events/s.

The acquired data is sent to the SHU data recorder on the satellite bus via SPI communication and then transmitted to the ground station sequentially. Commands related to the control of the INSPIRE sent from the ground station are received by the Raspberry Pi via serial communication and executed through the USB board.

The applied voltage of the MPPC is applied by the HV on the analog board. The power of the analog board is controlled by the mPDU, and it is turned off when a power control command is sent or in the event of an abnormal condition such as overcurrent.

The analog boards are connected in a ladder-like manner with synchronized clock signals, allowing the clocks of each analog board to be unified.

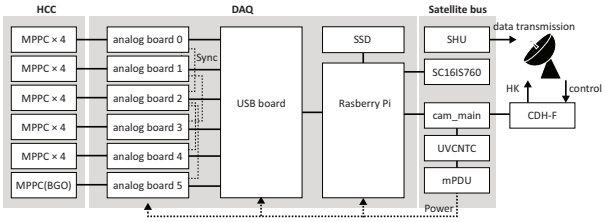

Figure 2: INSPIRE system diagram and communication with the satellite bus. The obtained event data is digitized by the analog board, aggregated by the USB board, and saved to the SSD by the Raspberry Pi. The Raspberry Pi communicates and transfers data with the ground station via the Satellite Bus

4 Performance test for each layers

Imaging tests using a ^{137}Cs source were conducted for the Scatterer, Side Absorber, and Bottom Absorber. Figure 3, 4 shows the imaging results for the Scatterer and Side Absorber when focusing on the energy condition of 662 keV gamma rays. The scintillation of each 45 × 45 pixel scintillator array can be observed, confirming the optical bonding between the scintillators and MPPCs is successful.

Figure 5 shows the output correlation diagram between the top and bottom MPPCs in the Bottom Absorber. Four scintillators are sandwiched between the two MPPCs through an air layer, and the scintillation from each scintillator is sufficiently separated. The imaging for events corresponding to 662 keV gamma rays in each layer is shown in figure B), where the scintillation of each scintillator array in each layer can be observed, confirming the acquisition of two-dimensional imaging and depth information.

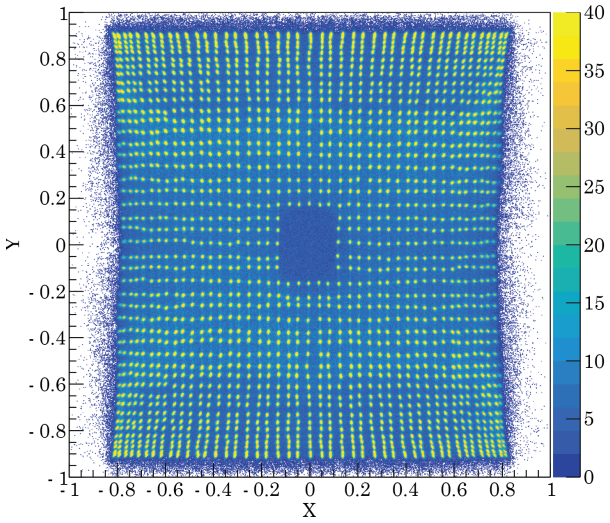

Figure 3: Imaging result of the Scatterer using a ^{137}Cs source. A two-dimensional distribution was reconstructed for events corresponding to the energy condition of 662 keV gamma rays. The scintillation of each 45×45 pixel scintillator can be observed, confirming the consistent and successful optical bonding between the scintillators and MPPCs. The structure of the hole for pinhole mode can beseen in the center of the scintillator.

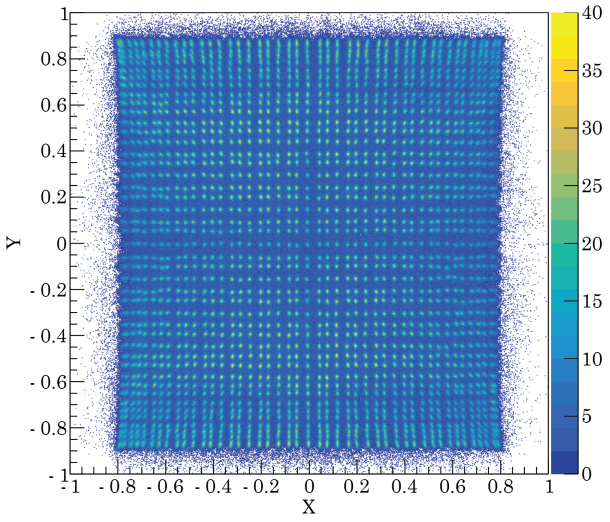

Figure 4: Imaging result of the Side Absorber using a ^{137}Cs source. The measurement conditions are the same as in Fig. 4.

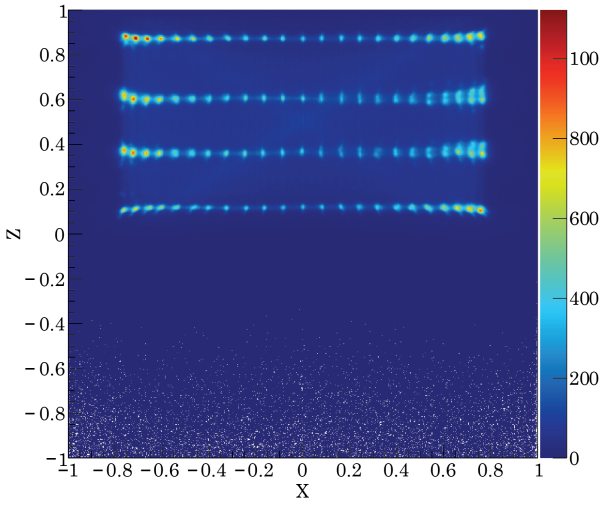

Figure 5: Imaging result of the Bottom Absorber using a ^{137}Cs source. The measurement conditions are the same as in Fig. 5. The Y-axis represents the depth direction obtained using the two MPPC arrays, while the X-axis represents the X direction in two-dimensional imaging. Since four scintillators are sandwiched through an air layer, the scintillation of each scintillator layer can be observed separately.

5 Performance Evaluation

5.1 Intrinsic Efficiency and Angular Resolution

By irradiating monochromatic energy from the front onto the geometry reproduced on Geant4,[11] we calculated the intrinsic efficiency and angular resolution of the pinhole mode and Compton mode in the range of 50 keV-500 keV and 200 keV-3 MeV, respectively. Intrinsic efficiency in pinhole mode was calculated as the gamma-ray events satisfying energy conditions that "pass through the hole" and "interact only in the absorber" (Fig. 6). In Compton mode, intrinsic efficiency was calculated for gamma-ray events that met energy conditions and were simultaneously detected by scatterer+bottom absorber or scatterer+side absorber.

In pinhole mode, intrinsic efficiency peaked at 100 keV at 0.5 %. Below 100 keV, sensitivity decreases as low-energy gamma rays interact with the MPPCs located directly behind the hole or absorber. Above 100 keV, sensitivity decreases as Compton scattering events in the absorber increase. In Compton mode, sensitivity decreases as escape events passing through the INSPIRE increase with higher energy.

Angular resolution in pinhole mode significantly surpasses that of COMPTEL, while it is comparable in Compton mode (Fig. 7). The position resolution of the detection unit is a few mm for the INSPIRE compared to a few cm for COMPTEL's 1.7 m distance between detection units.[?] Therefore, similar angular resolution is achieved. Since the angular resolution in both modes is at most a few degrees, the attitude control accuracy of the satellite is almost negligible.

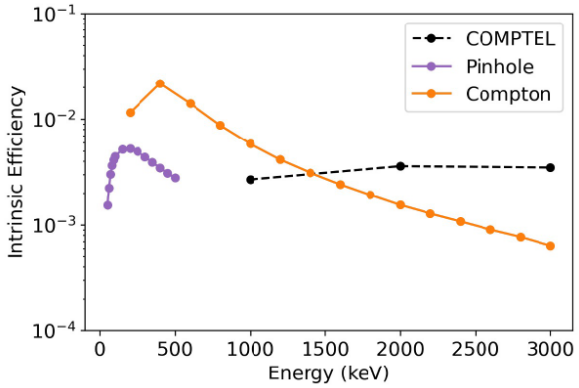

Figure 6: Comparison of intrinsic efficiency in pinhole mode and Compton mode with COMPTEL.

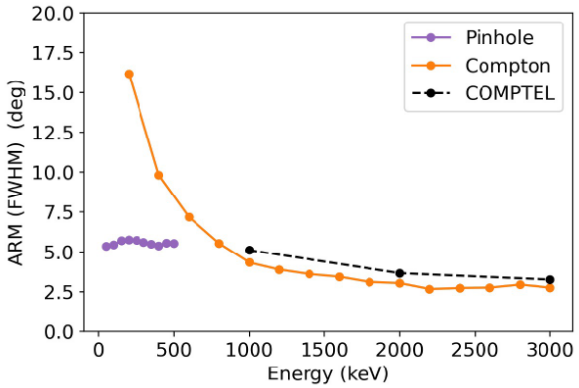

Figure 7: Comparison of angular resolution in pinhole mode and Compton mode with COMPTEL.

5.2 Continuum Sensitivity and Line Sensitivity

The continuum sensitivity $S(E)$ [ph cm^{-2} s^{-1} keV^{-1}] is calculated by the following formula.

$$S(E) = \frac{f}{\eta(E)}\sqrt{\frac{b(E)}{A\Delta ET}} \quad (1)$$

Here, f is the detection limit σ, $\eta(E)$ is the intrinsic efficiency, $b(E)$ [cnt cm^{-2} s^{-1} keV^{-1}] is the background detected by the detector, A [cm^2] is the detector area, ΔE is the energy width to be integrated, and T [s] is the exposure time. For both pinhole and Compton modes, assuming $f = 3\sigma$, $A = 100$ cm^2, $\Delta E = E$, and $T = 10^6$ and 3.6×10^7, continuum sensitivity was calculated.

Below several hundred keV, CXB dominates, and above that, Albedo gamma-rays dominate. For pinhole mode, CXB was assumed, and for Compton mode, Albedo gamma-rays were assumed to simulate $b(E)$ (Fig. 8). The assumed spectral shapes are summarized in Table 2.

Line Sensitivity $S(E)$ [ph cm^{-2} s^{-1} keV^{-1}] is calculated by the following formula.

$$S(E) = \frac{f}{\eta(E)}\sqrt{\frac{2b(E)\delta E}{AT}} \quad (2)$$

Here, δE is the energy resolution of the detector. Assuming $f = 3$, $A = 100$ cm^2, $\delta E = 9\%$ (FWHM) at 662 keV, $T = 10^6$, 2.4 x 10^7 s, the line sensitivity is shown in Fig. 9. The same simulated values of $\eta(E)$ and $b(E)$ were used as for the continuum sensitivity derivation. The line sensitivity of INSPIRE is comparable to that of the COSI satellite, a gamma-ray observation satellite planned by NASA for the MeV gamma-ray range, below several hundred keV.[12]

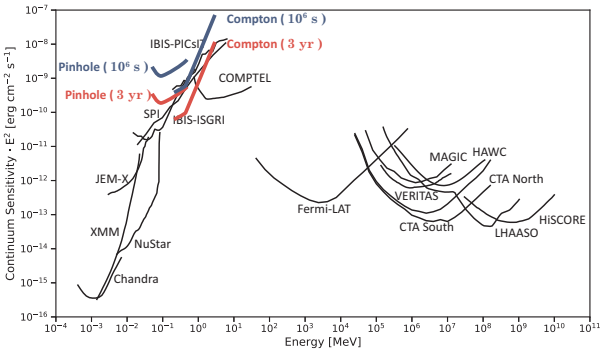

Figure 8: Comparison of continuum sensitivity for X-ray and gamma-ray in various projects.[13]

Table 2: Assumed spectral shape for Crab Nebula observation

Parameter	Crab	CXB	Albedo
Energy range	50 keV-10 MeV	50 keV-10 MeV	50 keV-100 MeV
Photon Index Γ	-2.2	-2.88	-1.35
Flux [ph cm^{-2} s^{-1} keV^{-1}]	4×10^{-6}	5×10^{-5}	5×10^{-4}

CXB, Albedo fluxes are assumed for $\Omega = 4\pi$ sr

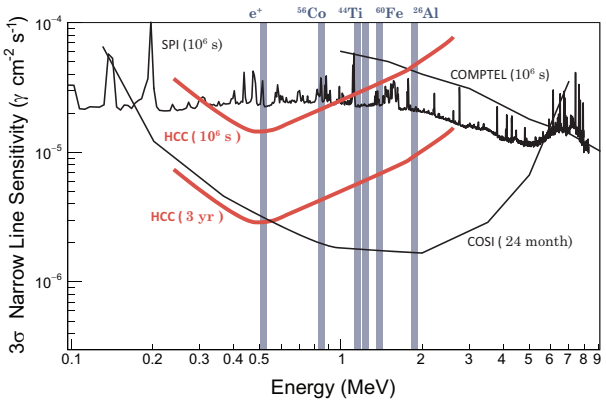

Figure 9: Comparison of line sensitivity for X-ray and gamma-ray in various projects.[14]

6 Environment testing

Since the data acquisition infrastructure consists of commercial off-the-shelf products from Hamamatsu Photonics not originally intended for use in space, we conducted thermal cycle testing and radiation resistance testing. Both tests confirmed that the components meet the operational requirements in the expected environments.

6.1 Thermal Environment Testing

We performed thermal soak tests to verify the components' resilience to expected low and high temperatures and thermal cycle tests to ensure they can withstand temperature variations in the anticipated orbital environment.

The thermal soak tests were conducted on the ADC board, USB board, and two Raspberry Pi units. One board was placed in a temperature-controlled chamber, and a test pulse simulating signals from the MPPC was input at 10 Hz (Fig. 10). We checked whether the board could correctly measure each pulse signal and whether the supplied voltage remained stable to ensure no overcurrent occurred, thereby confirming the board's thermal resistance. Thermocouples were attached to the key components of each board to monitor temperature during the tests. Initially, the power was turned on, and the temperature at each measurement point was allowed to stabilize at 20 °C. From this state, the temperature was increased to 85 °C at a rate of 10 °C per hour and then decreased back to 20 °C at the same rate. Throughout this sequence, all boards operated without issues, and pulse measurements were successfully performed.

For the thermal cycle test, we used the same measurement setup and cycled the temperature between -40 °C and 85 °C over 95 minutes, completing 15 cycles. All boards functioned properly throughout the 15 cycles.

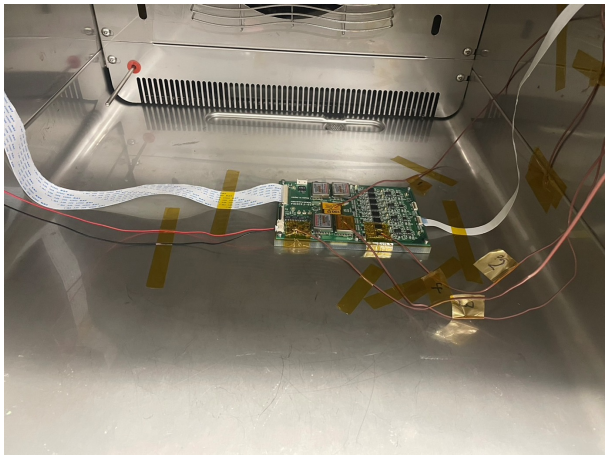

Figure 10: Setup for the thermal soak test of the analog board inside the temperature-controlled chamber. Thermocouples are attached to critical components, and test pulses are input, with the readout being sent to the USB board outside the chamber.

6.2 Radiation testing

As part of the radiation resistance testing for the analog board and USB board, we conducted tests for Single Event Upset (SEU) and Single Event Latch-up (SEL) caused by protons in satellite orbit using an 80 MeV proton beam. The proton beam profile was homogenized using the wobbler method, and the irradiation field size was set to 2.4 cm in the x-direction and 5.0 cm in the y-direction, meeting the beam's standard conditions. During irradiation, test

pulse signals were input to evaluate the frequency of abnormal operation states, such as overcurrent. The beam positions were set to cover five elements: (1) FPGA and SRAM, (2) DDR2-SDRAM, (3) USB controller on the USB board, and (4) CPLD, (5) LSI on the ADC board. The beam intensity was adjusted between 2 to 5 nA based on the error frequency.

The test results are shown in Table 3. Assuming a sun-synchronous orbit, the flux of 80 MeV protons is approximately ≈ 10 cm^{-2}s^{-1}. The table lists the equivalent elapsed years on an orbital satellite based on the fluence irradiated over an area of 50 cm^2. It was found that errors caused by protons would occur roughly once every few months on orbit. However, it is possible to avoid critical issues by immediately cutting the power and taking appropriate actions when an anomaly occurs.

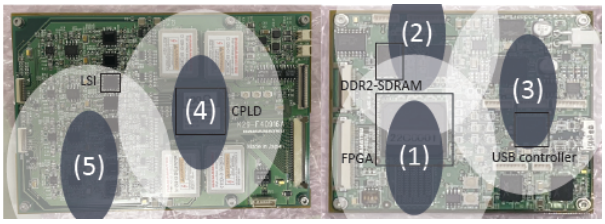

Figure 11: Spot positions irradiated with proton beams during the radiation resistance testing. The blue area indicates the region where the beam flatness is within ±4%, while the white area represents the region with more than half of the beam flux at the center.

7 Conclusion

The GRAPHIUM satellite is being developed as the successor to PETREL, which is currently being prepared for launch, with a planned launch in 2027. The INSPIRE has completed the construction of the communication interface with the satellite bus, and the command system for communication is being formulated. Temperature and radiation resistance tests have already been conducted on unit-level components. Based on these tests, the INSPIRE EM unit has been completed, and performance evaluation at the practical level will proceed.

8 Acknowledgments

This research was supported by the Japan Science and Technology Agency (JST) ERATO Grant No. JPMJER2102.

References

[1] M. R. Drout et al. Light curves of the neutron star merger gw170817/sss17a: Implications for r-process nucleosynthesis. *Science*, 358(6370):1570–1574, 2017.

[2] V. Schonfelder et al. The imaging compton telescope comptel on the gamma ray observatory. *IEEE Transactions on Nuclear Science*, 31(1):766–770, 1984.

[3] V. Schoenfelder et al. Instrument Description and Performance of the Imaging Gamma-Ray Telescope COMPTEL aboard the Compton Gamma-Ray Observatory. , 86:657, June 1993.

[4] J. Kataoka et al. Inspire: challenge of 50kg satellite to open up mev gamma-ray astronomy. In *HSTD13*, 2023.

[5] R. Iwashita et al. Design and evaluation of a mev gamma-ray camera aboard a 50-kg class small satellite. In *HSTD13*, 2023.

[6] Y. Yatsu et al. *Annual Small Satellite Conference*, 86:657, 2023.

[7] K. Watanabe et al. Concept design and development of 30kg microsatellite hibari for demonstration of variable shape attitude control. In *34th Annual Small Satellite Conference*, volume SSC19-VII-02, 2020.

[8] H. Kobayashi et al. Petrel for astrophysics and carbon business. In *37th Annual Small Satellite Conference*, volume SSC23-WIV-07 of *37th Annual Small Satellite Conference*, 2023.

[9] E. Kuriyama et al. Compton camera imaging of a gamma-ray glow from a thunderstorm. *Geophysical Research Letters*, 49(19):e2022GL100139, 2022. e2022GL100139 2022GL100139.

[10] N. Koshikawa et al. Activation imaging of drugs with hybrid Compton camera: A proof-of-concept study. *Applied Physics Letters*, 121(19):193701, 11 2022.

[11] S. Agostinelli et al. Geant4—a simulation toolkit. *Nuclear Instruments and Methods in Physics Research Section A: Accelerators, Spectrometers, Detectors and Associated Equipment*, 506(3):250–303, 2003.

[12] John A. Tomsick et al. The compton spectrometer and imager project for mev astronomy, 2021.

Table 3: Results of radiation resistance testing. The table summarizes the number of cases where overcurrent occurred and did not occur in instances where normal measurements could not be performed.

No.	Board	Components	Total Irradiation Years (yr)	Overcurrent	No Overcurrent
(1)	USB board	FPGA, SRAM	2.7	3	0
(2)	USB board	DDR2-SDRAM	1.0	1	1
(3)	USB board	USB controller	0.4	0	1
(4)	Analog board	CPLD	8.0	0	0
(5)	Analog board	LSI	7.0	0	0

[13] Giulio Lucchetta et al. Introducing the mevcube concept: a cubesat for mev observations. *Journal of Cosmology and Astroparticle Physics*, 2022(08):013, aug 2022.

[14] Julie McEnery et al. All-sky medium energy gamma-ray observatory: Exploring the extreme multimessenger universe, 2019.